Using GRACE to Explain Variations in the Earth's Oblateness

Sun, Yu; Riva, Riccardo; Ditmar, Pavel; Rietbroek, Roelof

DOI
10.1029/2018GL080607

Publication date
2019

Document Version
Final published version

Published in
Geophysical Research Letters

Geophysical Research Letters

RESEARCH LETTER
10.1029/2018GL080607

Using GRACE to Explain Variations in the Earth's Oblateness

Yu Sun[1,2], Riccardo Riva[2], Pavel Ditmar[2], and Roelof Rietbroek[3]

[1]Key Laboratory of Data Mining and Sharing of Ministration of Education, Fuzhou University, Fuzhou, China, [2]Department of Geoscience and Remote Sensing, Delft University of Technology, Delft, Netherlands, [3]Institute of Geodesy and Geoinformation, University of Bonn, Bonn, Germany

Key Points:
- The proposed approach allows to both estimate and interpret the J_2 time series
- The obtained data-driven time series of J_2 variations is consistent with SLR solutions
- Interannual J_2 variations are primarily explained by mass variations in atmosphere, oceans, and land waters

Supporting Information:
- Supporting Information S1
- Data Set S1

Correspondence to:
Y. Sun,
yusun@fzu.edu.cn

Citation:
Sun, Y., Riva, R., Ditmar, P., & Rietbroek, R. (2019). Using GRACE to explain variations in the Earth's oblateness. *Geophysical Research Letters*, *46*, 158–168. https://doi.org/10.1029/2018GL080607

Received 24 SEP 2018
Accepted 23 DEC 2018
Accepted article online 3 JAN 2019
Published online 15 JAN 2019

Abstract We present a new approach to estimate time variations in J_2. Those variations are represented as the sum of contributions from individual sources. This approach uses solely Gravity Recovery And Climate Experiment (GRACE) data and the geoid fingerprints of mass redistributions that take place both at the surface and in the interior of the solid Earth. The results agree remarkably well with those based on satellite laser ranging, while estimates of the sources explain the observed variations in J_2. Seasonal variations are dominated by terrestrial water storage and by mass redistribution in the atmosphere and ocean. Trends, however, are primarily controlled by the Greenland and Antarctic ice sheets and by glacial isostatic adjustment. The positive trend from surface mass variations is larger than the negative trend due to glacial isostatic adjustment and leads to an overall rising trend during the GRACE period (2002–2017).

Plain Language Summary J_2 variations indicate changes in the flattening of the Earth, which are mainly due to the Earth's response to large-scale mass redistribution at its surface and related to ongoing climate change. Though monitored over four decades by Earth observations satellites, the contributing sources to J_2 variations have not yet been accurately constrained, mostly due to deficiencies in geophysical models. In this study, we propose an approach to simultaneously estimate and interpret J_2 temporal variations based on gravity observations from the Gravity Recovery And Climate Experiment satellite mission. We reconstruct the observed gravity changes by a superimposition of spatial patterns characteristic of individual sources. We find that the seasonal and interannual variations are well explained by mass changes in atmosphere, oceans, and land water storage. The secular trend, on the other hand, is mainly caused by ice sheet melt, which has a positive effect (causing the Earth to be flatter), and by the ongoing solid Earth response to past glaciations, which has a negative trend (causing the Earth to be rounder). The trend due to ice sheet melting during 2002–2017 has a larger absolute value, so that the overall trend is rising, and the Earth is currently becoming flatter.

1. Introduction

J_2, also known as the Earth's dynamic oblateness, is a fundamental parameter affecting the Earth's rotational behavior. Its time variations, ΔJ_2 (hereafter denoted as J_2 for simplicity), are driven by latitudinal large-scale mass redistributions in the Earth system, which are intimately associated with ongoing climate change (e.g., Cox & Chao, 2002; Dickey et al., 2002), as well as with geodynamic processes inside the solid Earth (Benjamin et al., 2006).

For more than four decades, J_2 has been monitored by satellite laser ranging (SLR; Cheng et al., 2013). In the last 20 years, new data types, platforms, and methodologies have become available, and this enables comparisons between different solutions (Meyrath et al., 2017). Under the assumption that the Earth deforms elastically (Blewitt, 2003), seasonal J_2 variations can be derived from Global Positioning System-detected solid Earth deformations (Gross et al., 2004; Lavallée et al., 2010) or Earth's rotation variations (Chen & Wilson, 2003). However, a consideration of only elastic Earth's properties implies that viscoelastic solid Earth signals, such as glacial isostatic adjustment (GIA), are ignored. As a consequence, linear trends in J_2 cannot be reliably estimated. The recently ended Gravity Recovery And Climate Experiment (GRACE) satellite mission monitored changes in the Earth's gravity field for almost 15 years (Tapley et al., 2004). This includes the observation of J_2, which is directly related to the degree-2 zonal (C_{20}) coefficient of the gravity

field ($J_2 = -\sqrt{5}C_{20}$). Unfortunately, GRACE estimates of J_2 variations are generally less accurate than those based on SLR observations (e.g., Bonin et al., 2018; Chen & Wilson, 2008; Talpe et al., 2017), partly due to thermal-dependent systematic errors in the accelerometers onboard the GRACE satellites (Cheng & Ries, 2017). Sun, Ditmar, and Riva (2016) have demonstrated that a sufficiently accurate J_2 time series can be obtained from GRACE data supported by an oceanic C_{20} coefficient time series, derived from ocean bottom pressure (OBP) variations by an ocean circulation model (Meyrath et al., 2017). This approach, which is an extension of the method by Swenson et al. (2008), will be from here on referred to as the GRACE-OBP approach. It has been further refined by using better parameter settings (Sun et al., 2016) and incorporating information about errors in the input data sets (Sun et al., 2017). It is important to note that the trend estimates obtained with the GRACE-OBP approach contain, among others, the contribution provided by GIA models. Those models, however, are believed to carry large uncertainties.

The J_2 time series is composed of not only a linear trend but also a prominent annual cycle, as well as other signals with other periods, including long-term ones. The linear trend is mainly due to a combination of GIA effects (Yoder et al., 1983) and ongoing mass loss of the ice sheets (Nerem & Wahr, 2011), while the annual cycle is primarily caused by mass redistribution within atmosphere, oceans, and land hydrology. Other signals, including multiple year (2–7 years) and decadal variations, are also recognizable (Cheng & Ries, 2018) but still not fully explained due to deficiencies of existing geophysical models (Chen et al., 2016). Variations at periods longer than 1 year are especially interesting as the superposition of such signals can be strong enough to temporally reverse the secular trend (Cheng & Tapley, 2004; Cox & Chao, 2002). A notable example is the "1998 anomaly" (Cox & Chao, 2002). This anomaly has been reproduced by a superposition of anomalies of land water, oceans, and atmosphere variations (Dickey et al., 2002; Lavallée et al., 2010) and by a combination of decadal variations and El Niño–Southern Oscillation-related interannual variations (Cheng & Ries, 2018; Cheng & Tapley, 2004). Alternatively, it can be partly attributed to mismodeling of the Earth body tide (with a period of 18.6 years; Benjamin et al., 2006). Therefore, a definitive explanation of the "1998 anomaly" is still lacking.

A novel way to interpret temporal variations of the Earth's gravity field was proposed by (Rietbroek et al., 2012, 2016). Their approach employs prescribed normalized geoid change patterns associated to regional mass redistributions as basis functions, also known as fingerprints (see more information in Text S1 in the supporting information). As input, variations of the Earth's gravity and sea level are used. The observations of those variations are provided by GRACE and satellite altimetry, respectively. This approach gives insight not only into gravity filed variations but also into regional sea level variations. Furthermore, the authors have demonstrated the ability of this approach to estimate degree-1 variations of the Earth's gravity field, which are directly related to geocenter motion (Blewitt, 2003).

In this paper, we extend the work of Rietbroek and colleagues in order to retrieve J_2 variations. We show that this approach allows for not only an estimation but also for direct interpretation of the observed J_2 variations. Such an approach will be referred as the fingerprint approach (FPA) hereafter.

2. Methodology

2.1. Fingerprint Database

We define the base functions in line with Rietbroek et al. (2016). Each base function is defined as a geoid fingerprint associated with a particular spatial mass distribution. To that end, the sea level equation on an elastic Earth is solved (Farrell & Clark, 1976; Kendall et al., 2005; Tamisiea et al., 2010). First, we define two types of mass distribution over land areas: ice-related and hydrology-related ones. The former accounts for ice mass variations over the Antarctic ice sheet (AIS), the Greenland ice sheet (GIS), and glaciers (GLA). They are obtained by splitting land areas into geographical regions, assuming that a unit mass is distributed uniformly over each of those regions. The hydrology-related mass distributions are associated with terrestrial water storage (TWS) variations, which reflect the global water cycle. At that stage, we use the same mass distributions as described in Rietbroek et al. (2016). They were derived from the WaterGAP Hydrology Model (WGHM; e.g., Müller Schmied et al., 2014, 2016) by applying the empirical orthogonal function (EOF) analysis (Monahan et al., 2009; North, 1984). A unit mass is then distributed following the spatial pattern prescribed by a given EOF mode. In addition, we define GIA-related mass distributions to account

for the solid Earth contribution. We do not estimate the atmosphere and dynamic ocean effects (AO), since they are largely removed from GRACE level 2 data product by means of the Atmosphere and Ocean Dealiasing (AOD) product (RL05 or RL06; Dobslaw et al., 2017; Flechtner & Dobslaw, 2013).

We divided the AIS and the GIS into drainage systems following the definition of the Goddard Ice Altimetry Group (Zwally et al., 2012). The AIS consists of 27 drainage systems (Figure S1). The GIS is divided into eight drainage systems, each being further divided into two regions separated by the 2,000-m elevation line, for a total of 16 regions (Figure S2). Each of the regions defined within the AIS and GIS is associated with one fingerprint. For GLA, we use glacier positions archived by the National Snow and Ice Data Center through the Global Land Ice Measurements from Space project (Kargel et al., 2014). We separate the global set of glaciers into 50 groups (Figure S3). For each group, the mass variation pattern is proportional to the number of glaciers per $1° \times 1°$ grid cell (Figure S4). Note that we also model glaciers along the coastlines of Greenland and Antarctica, as many of them are not a part of the ice sheet drainage systems. In particular, large residual signals are seen if fingerprints representing the Greenland peripheral glaciers are ignored (Rietbroek et al., 2016). Over Antarctica, the effect of considering peripheral glaciers is much smaller. An exception is the Totten Glacier. Though located inside a drainage system, this glacier definitely needs a dedicated fingerprint, due to its large mass loss (Mohajerani et al., 2018). To simplify the analysis of the obtained results, we categorize all the glaciers into three large groups, the Greenland peripheral glaciers (GLA-GRE), the Antarctic peripheral glaciers (GLA-ANT), and the rest of the continental glaciers (GLA-CON). The estimated changes in GLA-GRE and GLA-ANT should be added to GIS and AIS, respectively, to obtain the total contribution of Greenland and Antarctica to J_2 variations. To compute the hydrology-related fingerprints, we select the 60 leading EOFs (explaining over 90% of the signal variance). Additionally, we create fingerprints for the Caspian Sea and the North India plains assuming the uniform mass distribution in both cases. The former addresses inconsistency between the WGHM predictions and GRACE observations; the latter accounts for large TWS changes due to human activities such as groundwater extraction. Both are not (well) represented by the WGHM model.

Finally, we pay special attention to creating GIA fingerprints. In total, we define six GIA fingerprints, which are associated with Laurentide, Fennoscandian, and Antarctic ice sheets. Based on the ICE-6G ice history model (Peltier et al., 2015), we create three regional GIA fingerprints for the Laurentide ice sheet and two fingerprints for the Fennoscandian ice sheet (Figure S5), in order to allow for the possible presence of regional biases in the input GIA model. For Antarctica, we create only one fingerprint for the entire territory. It is based on the IJ05 ice history (Ivins & James, 2005), which has been shown to provide the closest agreement to a data-driven GIA solution (Riva et al., 2009). The viscosity model used to generate the GIA fingerprints has a higher value in the lower mantle (10^{22} Pa s) than VM5a (Peltier et al., 2015), in line with results from a joint inversion of GIA and mantle convection observables (Mitrovica & Forte, 1997). More information about preparing regional GIA models can be found in supporting information (Text S2). Further more, we include two fingerprints representing the C_{21} and S_{21} coefficients to account for any possible errors in modeling the Earth's rotational feedback (e.g., Martinec & Hagedoorn, 2014; Mitrovica & Wahr, 2011). Altogether, we are using 163 fingerprints (Data Set S1).

2.2. Inversion Approach

Our approach uses the fingerprints as basis functions to represent the geoid changes observed by GRACE. Once the fingerprint database is built, we can estimate the scaling factors α^{f^i} associated to each fingerprint and needed to reproduce the observed geoid changes via

$$\underset{(k-5)\times k}{\mathbf{T}} \quad \underset{k\times n}{\mathbf{F}} \quad \underset{n\times 1}{\boldsymbol{\alpha}} = \underset{(k-5)\times 1}{\mathbf{g}}, \tag{1}$$

where $\mathbf{F}$ is a matrix of spherical harmonic analysis with n columns. Each column represents an individual fingerprint expressed in the spectral domain with k spherical harmonic coefficients starting from C_{00} (the unique index of each coefficients is given by $l^2 + i \times l + m + 1$, where l and m represent the degree and order, respectively; i equals 0 if $m = 0$ and 1 otherwise). $\mathbf{g}$ is the GRACE-based gravity field for a given month starting from C_{21}. The C_{00}, degree-1, and C_{20} coefficients are omitted, so that the length of vector $\mathbf{g}$ is $(k - 5)$. $\mathbf{T}$ is a truncation matrix used to account for the lacking coefficients in $\mathbf{g}$

$$\mathbf{T} = \begin{bmatrix} 0 & 0 & 0 & 0 & 1 & 0 & \dots & \dots & 0 \\ 0 & 0 & 0 & 0 & 0 & 1 & \ddots & \ddots & \vdots \\ \vdots & \vdots & \vdots & \vdots & \vdots & \ddots & \ddots & \ddots & \vdots \\ \vdots & \vdots & \vdots & \vdots & \vdots & \ddots & \ddots & 1 & 0 \\ 0 & 0 & 0 & 0 & 0 & \dots & \dots & 0 & 1 \end{bmatrix}. \quad (2)$$

An explicit form of equation (1) can be found in Text S3.

Vector α contains n unknowns (one for each fingerprint in a particular month) that are estimated by least squares

$$\boldsymbol{\alpha} = (\mathbf{F}^{\mathbf{T}}\mathbf{T}^{\mathbf{T}}\mathbf{P}\mathbf{T}\mathbf{F})^{-1}\mathbf{F}^{\mathbf{T}}\mathbf{T}^{\mathbf{T}}\mathrm{Pg}, \quad (3)$$

where **P** is a diagonal weight matrix with elements inversely proportional to the calibrated error variances of GRACE coefficients (downloaded from ftp://ftp.csr.utexas.edu/outgoing/grace/). Equation (3) gives an individual monthly GRACE solution; a time series of α can ultimately be obtained in this way for each fingerprint. It is worth noting that the scaling factors related to surface mass fingerprints are estimated without constrains, whereas those related to the GIA fingerprints need to be constrained in the time domain so that the resulting GIA-related J_2 components consist of only linear trends. An application of this constraint is facilitated by the fact that all coefficients of all months are estimated simultaneously. Readers are referred to the supporting information for more information (Text S4 and Figure S6). Once the scaling factors α^{f^i} have been determined, they are used to scale the C_{20} coefficients of each fingerprint. After that, the contributions of individual fingerprints are added together, allowing us to determine monthly variations in J_2. Note that the resulting J_2 solution is independent from the GRACE C_{20} coefficients but consistent with the rest of the GRACE solutions.

There is likely a certain degree of correlations between the GIA and the present-day mass transport (PDMT) trends at subregional scales, which could prevent an accurate separation of the different signals. However, PDMT fingerprints are representative of load changes occurring over much smaller regions than those of the GIA fingerprints, meaning that they are largely constrained by signals that are almost completely unrelated to GIA. This is also the reason that we are using a single GIA fingerprint for the whole of Antarctica. The ability of the inversion in Rietbroek et al. (2016) to separate GIA from the PDMT signals in Antarctica was limited. For that reason a constraint was applied that penalized large trend deviations from the apriori model. In this study, the applied regularization merely forces the GIA to a straight trendline, but it does not penalize its incline. Surprisingly, the current inversion does not show an instability to simultaneously estimated GIA and PDMT. The exact reasons are yet unknown, but we speculate that the use of diagonal error-covariance matrices in combination with the truncated set of Strokes coefficients acts as an implicit regularization with respect to to a full error-covariance model. Preliminary experiments based on significantly different GIA fingerpints show that the resulting J_2 trend varies less than 12% (see Text S5 and Table S1 for more information), which suggests that our inversion is fairly stable.

2.3. GRACE Data

The Center for Space Research (CSR) currently provides two releases of GRACE solutions: RL05 and the latest one RL06. Compared to RL05, RL06 is based on new background models, including an updated AOD data product, and new parameterization strategies. The AOD RL05 is based on the atmosphere model by the European Center for Medium-Range Weather Forecast (Dee et al., 2011) and the ocean model for circulation and tides (Thomas, 2002). The AOD RL06 (Dobslaw et al., 2017) makes use of the same atmosphere model but is based on a different ocean model, that is, the Max-Planck-Institute for Meteorology Ocean model (Jungclaus et al., 2013). In this study, we use both the CSR RL05 (Bettadpur, 2012) and CSR RL06 (Save, 2018) models completed to degree and order 60. In the RL05, the available solutions are from April 2002 to June 2017, while in the RL06 the available period is approximately 2 years shorter (January 2003 to August 2016). In the main text, we mainly show the results based on RL06, while the RL05 results are similar and can be found in the supporting information. A mean gravity field in the period covered by the GRACE data has been removed to isolate time variations of the gravity field. We did not apply any filtering/smoothing techniques. The pole tide correction (Wahr et al., 2015) is not applied as it has negligible effects on the resulting J_2 solutions. Also, such a correction is no longer needed for the CSR RL06 (F. Landerer, personal communication, October 24, 2018).

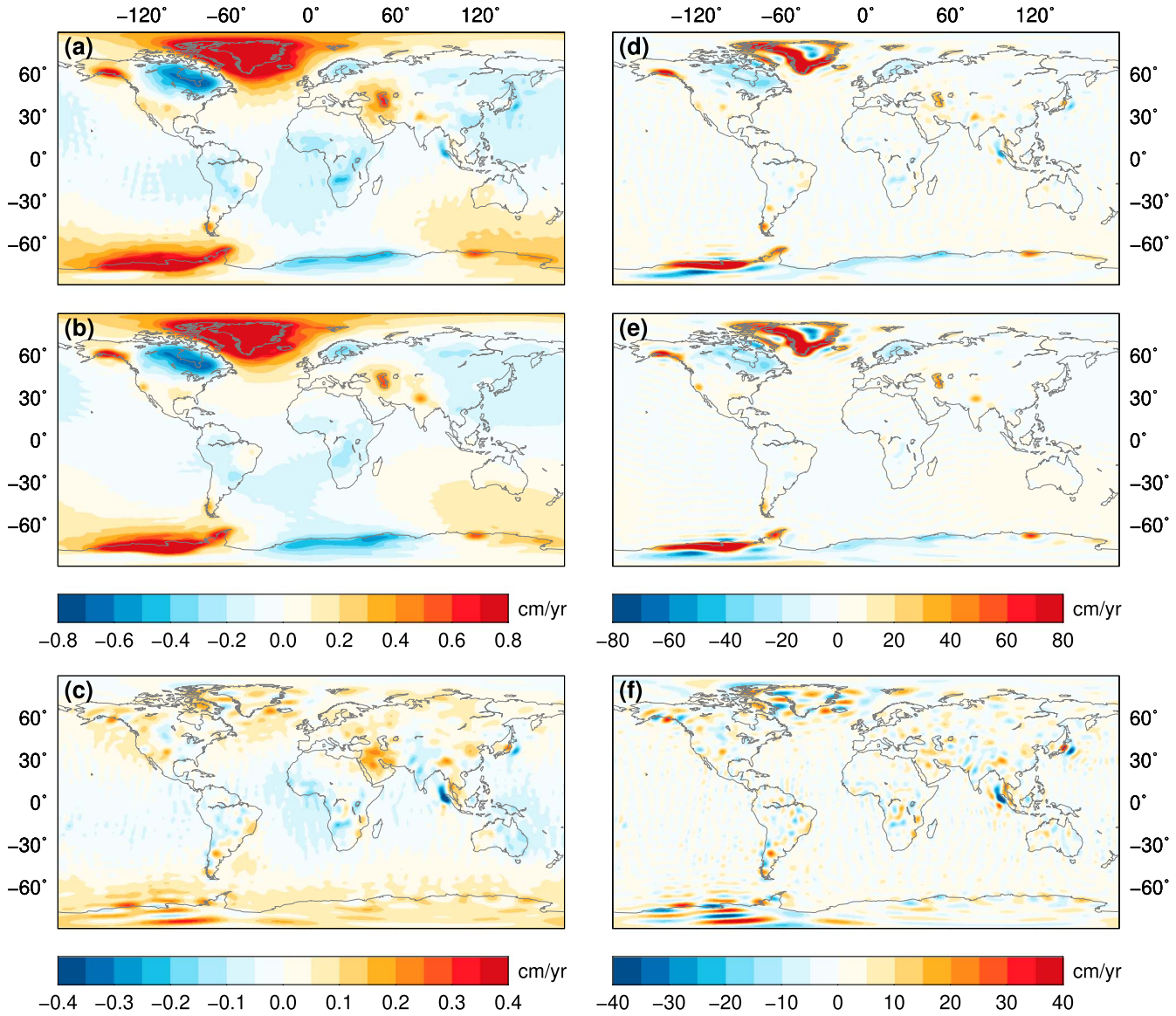

Figure 1. Global trend map in terms of geoid (a, b, c) and equivalent water height (d, e, f). Panels (a) and (d) show the results recovered with the original CSR RL06 solution. Panels (b) and (e) show those based on the fingerprint approach. Panels (c) and (f) show the residual signals between the two solutions (a, b and d, e). Notice the different color scales.

3. Results

We show in Figure 1a the global geoid trend estimated from the original CSR RL06 solutions, in Figure 1b the trend reconstructed by the fingerprints, and in Figure 1c the residuals between panels a and b. Additionally, we show in Figures 1d–1f the same results, represented in terms of equivalent water heights. The residual signals are rather small except for coseismic signals from megathrust earthquakes, such as the 2004 Sumatra Earthquake and the 2011 Tohoku Earthquake, as well as the signal around the Kamb Ice Stream in West Antarctica. These are expected because no earthquake-related fingerprints are prescribed in the database and because the large gradients in West Antarctica may not be well represented by uniform mass variations assigned to the drainage systems there. However, these signals only have minor effects on J_2 for their limited spatial scales. The only visible difference at large spatial scales is the band-shaped signal in Figure 1c, which shows that the inverted C_{20} coefficient is considerably different from the original GRACE C_{20} (Root Mean Square of residuals is 1.7×10^{-10}; Figure S7). The results for CSR RL05 are rather similar but with more noise (RMS of residuals is 3.0×10^{-10}; Figures S7 and S8).

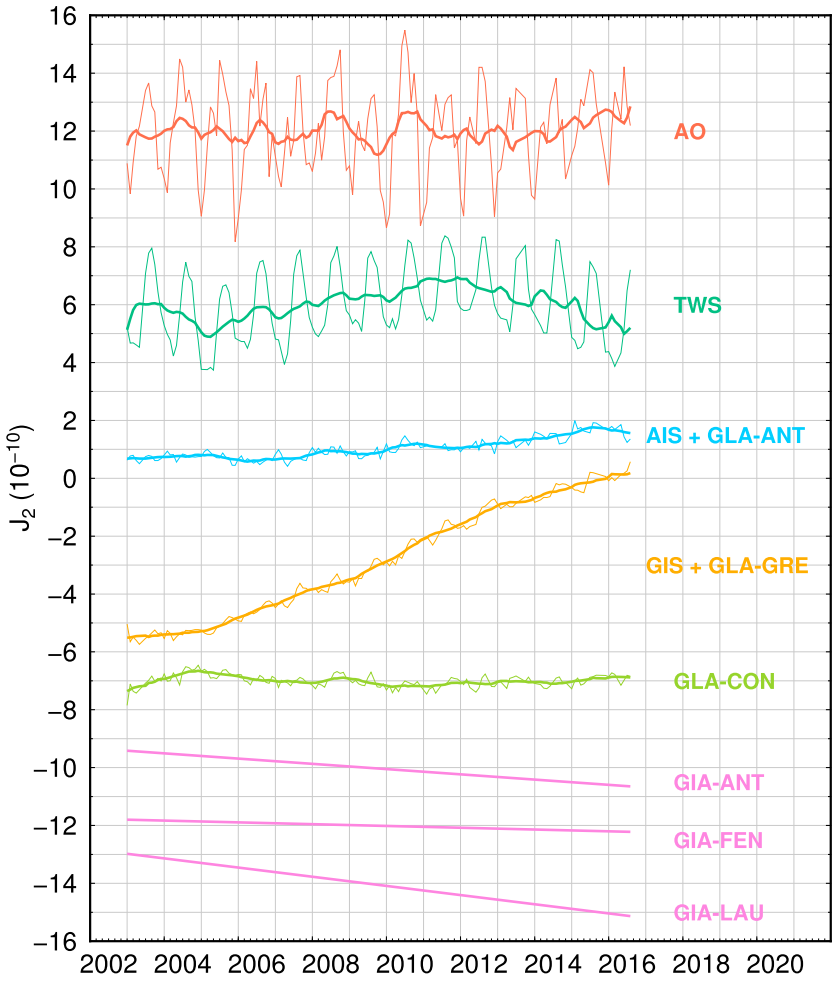

Figure 2. A comparison of J_2 estimates obtained from CSR RL06 data using the FPA approach (this study; red curve with dots) with those obtained using the GRACE-OBP approach (Sun et al., 2016; blue band), as well as with those based on SLR data (Cheng et al., 2013; gray band). An offset of (15×10^{-10}) is applied to the top pair of curves. Note that the SLR solution is represented by a gray band where the upper and lower bounds are defined by the $\mu \pm 2\sigma$ (μ denotes the mean values), respectively. The same is also applied to the GRACE-OBP solution, where the uncertainty ($\sigma = 1.13 \times 10^{-10}$) is calculated based on Ditmar et al. (2018). The error bars are also shown for the FPA solution. All three solutions represent the full J_2 signals, which means that the J_2 contributions from the atmosphere and dynamic ocean effects have been restored in the GRACE-based solutions. The differences between FPA and SLR as well as between FPA and GRACE-OBP are shown at the bottom of the plot with an offset of -20×10^{-10} being applied for clarity. The time series are based on the RL06 solutions, meaning that AOD RL06 product is adopted; the SLR solution uses AOD RL06 as background model. A RL05 version is available in the supporting information (Figure S9). CSR = Center for Space Research; FPA = fingerprint approach; GRACE = Gravity Recovery And Climate Experiment; OBP = ocean bottom pressure; SLR = satellite laser ranging.

In Figure 2 we plot the FPA and GRACE-OBP (Sun et al., 2016) estimates of J_2 based on CSR RL06 solutions, as well as the estimates based on SLR data (Cheng et al., 2013). A plot showing the estimates based on the CSR RL05 can be found in the supporting information (Figure S9). We calculate uncertainties of the FPA solution using the method developed by Ditmar et al. (2018). The 1σ interval (1.01×10^{-10}) is shown with black error bars: it is slightly larger than the RL05 version ($\sigma = 0.97 \times 10^{-10}$) and comparable with the SLR uncertainty, which has a mean value of 0.83×10^{-10} (computed from the uncertainties shown in the data file ftp://ftp.csr.utexas.edu/pub/slr/degree_2/RL06/C20_RL06_2018_04.txt). The differences between FPA and GRACE-OBP estimates (RMS: 0.44×10^{-10}) are smaller than those between FPA and SLR solution (RMS: 1.01×10^{-10}), indicating that the two GRACE-based estimates are consistent. Also, we notice that there is a linear trend left in the FPA/SLR differences from 2002 to 2008. The reasons for it remain unknown.

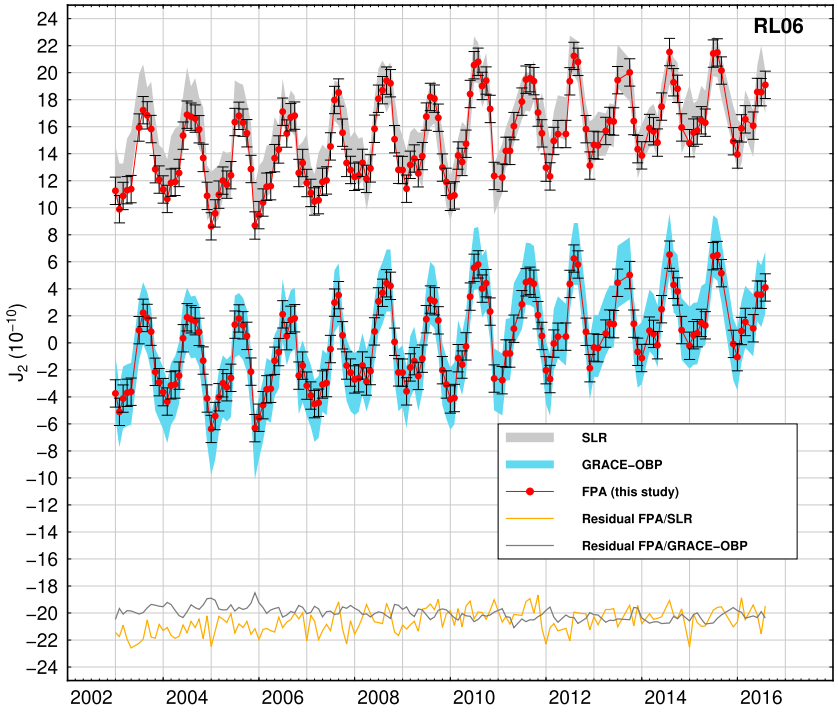

Figure 3. Contributions to the RL06 J_2 time serious estimated via the fingerprint approach. Offsets are applied for clarity. Note that the AO component is not estimated but directly taken from the AOD product. AIS + GLA-ANT and GRE + GLA-GRE represent the combined contributions of ice sheets and peripheral glaciers of Antarctica and Greenland, respectively. GLA-CON denotes the other continental galaciers. GIA-ANT, GIA-FEN, and GIA-LAU refer to the GIA effects due to Antarctica, Fennoscandian, and Laurentide ice sheets, respectively. Thick lines on top of the non-GIA components are the 11-month running means. AOD = Atmosphere and Ocean Dealiasing; AIS = Antarctica ice sheet; GLA-ANT = Antarctic peripheral glaciers; GRA-GLE = Greenland peripheral glaciers; GLA-CON = the rest of the continental glaciers; GIA = glacial isostatic adjustment; FEN = Fennoscandian; LAU = Laurentide.

All three J_2 solutions show dominant annual cycles. The annual amplitude of the FPA solution is virtually identical to that of the SLR solution (Table S2). In contrast, the annual amplitude of the GRACE-OBP solution is significantly larger (about 17%) and statistically different, though larger values are still in line with some other SLR estimates (Chen & Wilson, 2008; Cox & Chao, 2002). All three solutions also show significant semiannual variations (Table S2). They are comparable to each other within 2σ, as well as with those from some previous studies (Lavallée et al., 2010). Phase estimates for both annual and semiannual terms are insensitive to the time interval and consistent with each other within 1σ (annual) and 2σ (semiannual) range, which is about 1 and 2 weeks, respectively.

One of the main advantages of the FPA is that it allows one to separate the contributions of individual sources to the total signal. Here we separate the ice sheets, the glaciers, global land hydrology, and GIA (Figure 3). The AO contribution is not estimated by the FPA method but predicted by the AOD RL06 product. Note that it is almost the same as the one from RL05 (Figure S10), though they are based on different ocean circulation models. Clearly, the seasonal signals in J_2 are controlled by two components: AO and TWS. AO is the largest one with an annual amplitude of $1.85 \pm 0.10 \times 10^{-10}$, while TWS is slightly smaller with an annual amplitude of $1.27 \pm 0.07 \times 10^{-10}$. The combination of these two components explains almost the entire seasonal variations in J_2 (98% of the total signal variance; Table S3). However, both components have negligible contributions to the trend estimates over the whole time span (though a significant TWS trend is present over shorter periods).

It is clear that the rising trend in J_2 is mainly due to mass loss from GIS + GLA-GRE (0.44×10^{-10}). AIS + GLA-ANT also shows a positive trend of 0.07×10^{10}. GLA-CON, on the other hand, does not provide a significant contribution to the trend in J_2. Consistently with the fact that present-day GIA is causing large-scale uplifts at high latitudes, we see negative trends in all GIA-related sources, with the Laurentide GIA providing the largest contribution (-0.16×10^{-10}), followed by the Antarctica GIA (0.08×10^{-10}) and Fennoscandian

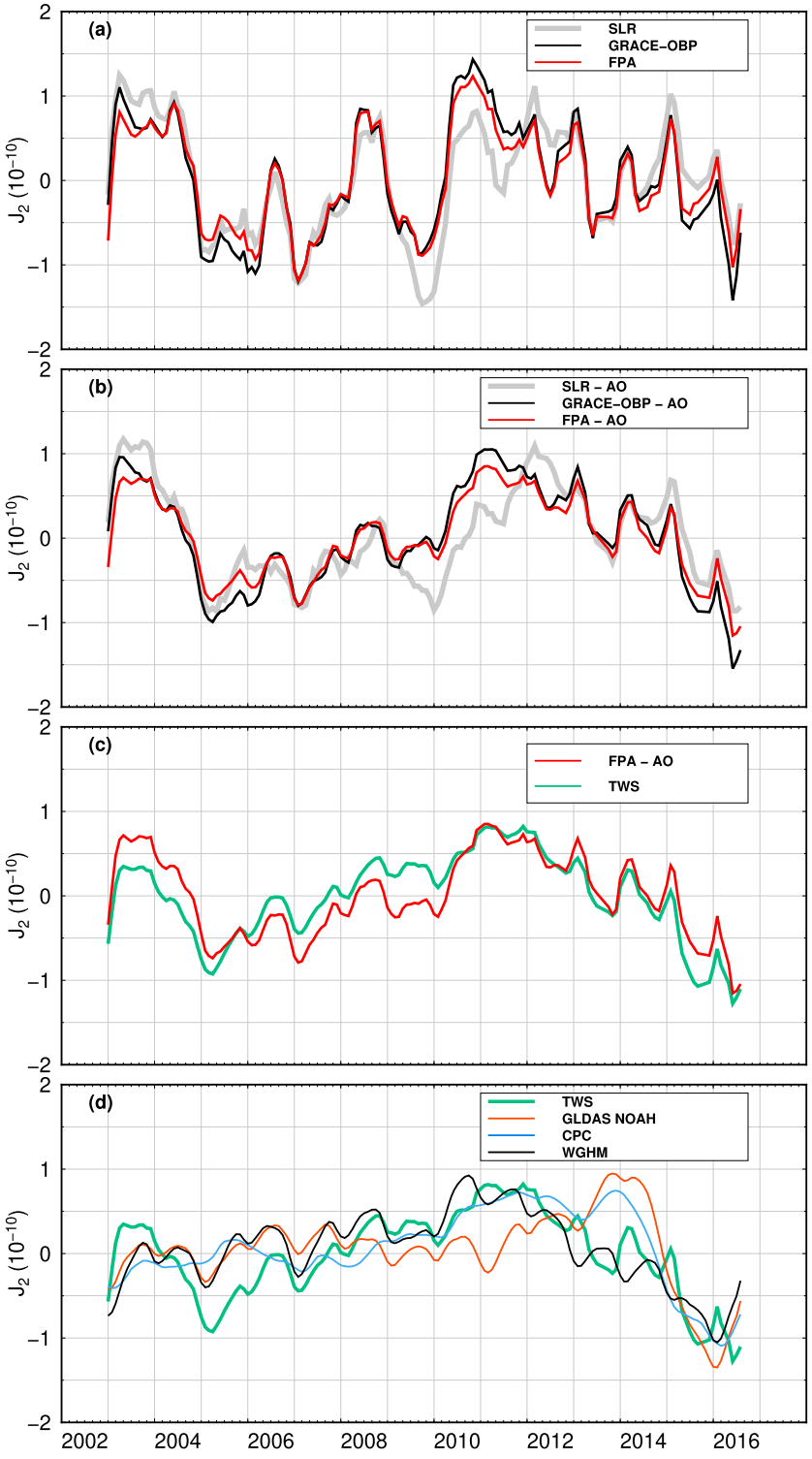

Figure 4. Interannual variations of the J_2 RL06 time series. (a) The comparison of J_2 solutions based on SLR data, GRACE-OBP approach, and this study. Note that these are the full J_2 time series with the AO component restored. (b) The residual J_2 signals without restoring the AO component. (c) The residual J_2 of this study with one of its contributing sources, that is, TWS. (d) The J_2 TWS component with those based on three hydrology models (a comparison with these three hydrological models at the seasonal time scale can be found in Text S5 and Figure S11). SLR = satellite laser ranging; GRACE = Gravity Recovery And Climate Experiment; OBP = ocean bottom pressure; TWS = terrestrial water storage; FPA = fingerprint approach; GLDAS-NOAH V1.0 = Global Land Data Assimilation System NOAH model; CPC = Climate Prediction Center model; WGHM = WaterGAP Hydrology Model.

GIA (-0.03×10^{-10}). In addition, the scaling factors for GIA fingerprints are provided in Data Set S2; the linear trends in those scaling factors are listed in Table S4.

In order to investigate interannual signals, we have computed 11-month running averages of the SLR, GRACE-OBP, and FPA detrended solutions. In Figure 4a, we see that the two GRACE-based solutions are close. The SLR solution is also generally aligned with the other two except for discrepancies during years 2009–2011. The AO component (Figure 3) explains a considerable part of the observed variability, which is particularly strong during 2008–2010 due to a major El Niño–Southern Oscillation event (Cheng & Ries, 2018) but certainly cannot account for all the variations. In Figure 4b, we show the residual J_2 time series (FPA-AO), that is, the one obtained prior to the restoration of the AO contribution, which is common to all solutions. Removing the AO contribution highlights even further the discrepancy between SLR and GRACE-based solutions during years 2009–2011. Most of the residual variability is well explained by the TWS component (Figure 4c); the correlation coefficient between the FPA-AO and the TWS is as high as 0.85. We further compare the FPA TWS component with predictions based on three hydrological models: the Global Land Data Assimilation System NOAH model (Rodell et al., 2004), the Climate Prediction Center model (Dool et al., 2003; Fan & Dool, 2004), and the WGHM (Müller Schmied et al., 2014, 2016; Figures 4d and S11). Note that the TWS fingerprints are based on an EOF analysis of WGHM, while the resulting amplitude is derived from GRACE data. But none of the hydrological models reproduces some features of the FPA solution, such as the low in 2005.

4. Discussions and Conclusions

The FPA is an effective approach to both explain and retrieve J_2 time series. According to the method proposed by Ditmar et al. (2018), the error in the FPA solution (approximately $\pm 1.0 \times 10^{-10}$) is comparable to that of the SLR solution (Cheng et al., 2013). Our solution suggests that the primary contributors to seasonal and interannual variations in J_2 over the GRACE period (2002–2017) are the AO and TWS components. The positive trend during this particular time interval is mainly due to mass loss from the ice sheets, particularly from Greenland, while contributions from mountain glaciers are minor.

The uniqueness of the FPA compared to other methods is that it helps understand the driving mechanisms of the observed time series. The traditional way of interpreting J_2 variations relies on the reconstruction of the observed signal by means of combining various of geophysical models. Unfortunately, some of the Earth's components, for example, mountain glaciers, are difficult to model due to rather sparse data constraints. Models for other components, such as GIA, often carry significant and unknown uncertainties. Also, there is no consensus on the choice of a hydrological model. Though many available, they typically lack some signals (particularly, of an anthropogenic origin). This limits their ability to explain all the mass variations observed with independent methods. Also, as noted by Lavallée et al. (2010) and Scanlon et al. (2018), geophysical models may be particularly weak in reconstructing multiple year variations. Our study also confirms a limited accuracy of existing hydrological models. We found that those models cannot fully explain the TWS contribution to our J_2 solution. Therefore, the estimated J_2 time series of different components from this study may be used to validate geophysical models in the future studies.

One may argue that our TWS component is estimated using base functions extracted from a hydrological model and thus should inherently carry uncertainties of that model. However, the FPA approach does not need a very accurate hydrology model to work because it rescales the original signals on a monthly basis. As long as a hydrology model can predict the major mass change patterns correctly, it should result in quite good J_2 solutions. The fact that we are only using the 60 leading EOFs is equivalent to a low-pass filtering the hydrology model. Therefore, the impact of missing small-scale mass changes is likely minor. We have verified, for instance, that removing the fingerprint for India plains, which is known to suffer from serious groundwater depletion, does not significantly alter the J_2 time series (RMS difference for the TWS-induced J_2 is 0.02×10^{-10}).

Finally, we have coestimated the geocenter motion (i.e., variations of degree-1 coefficients) simultaneously with C_{20} coefficient time series and compared it with the GRACE-OBP solution (Table S5 and Figure S12). A high accuracy of the GRACE-OBP solution has been proved by a few previous studies (Sun et al., 2017; Sun, Riva, & Ditmar, 2016; Zhang & Sun, 2018). Therefore, the close agreement of the two solutions provides a further support for the FPA approach.

Acknowledgments
We thank the anonymous reviewers for their constructive comments. We thank Hannes Müller Schmied for providing us with the WGHM model. An older version is available from http://www.uni-frankfurt.de/49903932/7_GWdepletion. Fingerprints created by Rietbroek are deposited in http://www.pangaea.de (doi: 10.1594/PANGAEA.855539). GRACE data were taken from the CSR website (http://www2.csr.utexas.edu/grace/) and the ICGEM website (http://icgem.gfz-potsdam.de/home). J_2 time series based on SLR analysis is downloaded from GRACE TELLUS (https://grace.jpl.nasa.gov/data/get-data/). CPC and GLDAS are publicly available (https://www.esrl.noaa.gov/psd/data/gridded/data.cpcsoil.html and https://disc.gsfc.nasa.gov/datasets?keywords=GLDAS). Fingerprints used in this study as well as their corresponding scaling factors for each months are submitted as data set in the supporting information. All results from this study will be made publicly available upon publication through the 4TU.Centre for Research Data (https://researchdata.4tu.nl/en/home/). Y. S. is supported by the National Natural Science Foundation of China (grant 41801393), the Education Department of Fujian Province (grant JT180031), and Central Guide Local Science and Technology Development Project (grant 2017L3012). He is also partially supported by the QiShan program of Fuzhou University. REMR acknowledges support by the Netherlands Organization for Scientific Research (NWO), through VIDI grant 864.12.012.

References

Benjamin, D., Wahr, J., Ray, R. D., Egbert, G. D., & Desai, S. D. (2006). Constraints on mantle anelasticity from geodetic observations, and implications for the J_2 anomaly. *Geophysical Journal International*, *165*(1), 3–16. https://doi.org/10.1111/j.1365-246X.2006.02915.x

Bettadpur, S. (2012). *UTCSR level-2 processing standards document*. Austin: Technical Version 4 Univ Texas.

Blewitt, G. (2003). Self-consistency in reference frames, geocenter definition, and surface loading of the solid Earth. *Journal of Geophysical Research*, *108*(B2), 2103. https://doi.org/10.1029/2002JB002082

Bonin, J. A., Chambers, D. P., & Cheng, M. (2018). Using satellite laser ranging to measure ice mass change in Greenland and Antarctica. *The Cryosphere*, *12*(1), 71–79. https://doi.org/10.5194/tc-12-71-2018

Chen, J. L., & Wilson, C. R. (2003). Low degree gravitational changes from earth rotation and geophysical models. *Geophysical Research Letters*, *30*(24), 2257. https://doi.org/10.1029/2003GL018688

Chen, J. L., & Wilson, C. R. (2008). Low degree gravity changes from GRACE, Earth rotation, geophysical models, and satellite laser ranging. *Journal of Geophysical Research*, *113*, B06402. https://doi.org/10.1029/2007JB005397

Chen, J. L., Wilson, C. R., & Ries, J. C. (2016). Broadband assessment of degree-2 gravitational changes from GRACE and other estimates, 2002-2015. *Journal of Geophysical Research: Solid Earth*, *121*, 2112–2128. https://doi.org/10.1002/2015JB012708

Cheng, M., & Ries, J. (2017). The unexpected signal in GRACE estimates of C_{20}. *Journal of Geodesy*, *91*(8), 897–914. https://doi.org/10.1007/s00190-016-0995-5

Cheng, M., & Ries, J. C. (2018). Decadal variation in Earth's oblateness (J2) from satellite laser ranging data. *Geophysical Journal International*, *212*(2), 1218–1224. https://doi.org/10.1093/gji/ggx483

Cheng, M., & Tapley, B. D. (2004). Variations in the Earth's oblateness during the past 28 years. *Journal of Geophysical Research*, *109*, B09402. https://doi.org/10.1029/2004JB003028

Cheng, M., Tapley, B. D., & Ries, J. C. (2013). Deceleration in the Earth's oblateness. *Journal of Geophysical Research: Solid Earth*, *118*, 740–747. https://doi.org/10.1002/jgrb.50058

Cox, C. M., & Chao, B. F. (2002). Detection of a large-scale mass redistribution in the terrestrial system since 1998. *Science*, *297*(5582), 831–833. https://doi.org/10.1126/science.1072188

Dee, D. P., Uppala, S. M., Simmons, A. J., Berrisford, P., Poli, P., Kobayashi, S., et al. (2011). The ERA-Interim reanalysis: Configuration and performance of the data assimilation system. *Quarterly Journal of the Royal Meteorological Society*, *137*(656), 553–597. https://doi.org/10.1002/qj.828

Dickey, J. O., Marcus, S. L., de Viron, O., & Fukumori, I. (2002). Recent Earth oblateness variations: Unraveling climate and postglacial rebound effects. *Science (New York, N.Y.)*, *298*(5600), 1975–1977. https://doi.org/10.1126/science.1077777

Ditmar, P., Tangdamrongsub, N., Ran, J., & Klees, R. (2018). Estimation and reduction of random noise in mass anomaly time-series from satellite gravity data by minimization of month-to-month year-to-year double differences. *Journal of Geodynamics*, *119*, 9–22. https://doi.org/10.1016/j.jog.2018.05.003

Dobslaw, H., Bergmann-Wolf, I., Dill, R., Poropat, L., Thomas, M., Dahle, C., et al. (2017). A new high-resolution model of non-tidal atmosphere and ocean mass variability for de-aliasing of satellite gravity observations: AOD1b RL06. *Geophysical Journal International*, *211*(1), 263–269. https://doi.org/10.1093/gji/ggx302

Dool, H. v. d., Huang, J., & Fan, Y. (2003). Performance and analysis of the constructed analogue method applied to U.S. soil moisture over 1981-2001. *Journal of Geophysical Research*, *108*(D16), 8617. https://doi.org/10.1029/2002JD003114

Fan, Y., & Dool, H. v. d. (2004). Climate Prediction Center global monthly soil moisture data set at 0.5 resolution for 1948 to present. *Journal of Geophysical Research*, *109*, D10102. https://doi.org/10.1029/2003JD004345

Farrell, W. E., & Clark, J. A. (1976). On postglacial sea level. *Geophysical Journal of the Royal Astronomical Society*, *46*(3), 647–667. https://doi.org/10.1111/j.1365-246X.1976.tb01252.x

Flechtner, F., & Dobslaw, H. (2013). AOD1b Product Description Document for Product Release. 05, GFZ German Research Centre for Geosciences.

Gross, R. S., Blewitt, G., Clarke, P. J., & Lavallée, D. (2004). Degree-2 harmonics of the Earth's mass load estimated from GPS and Earth rotation data. *Geophysical Research Letters*, *31*, L07601. https://doi.org/10.1029/2004GL019589

Ivins, E. R., & James, T. S. (2005). Antarctic glacial isostatic adjustment: A new assessment. *Antarctic Science*, *17*(04), 541–553. https://doi.org/10.1017/S0954102005002968

Jungclaus, J. H., Fischer, N., Haak, H., Lohmann, K., Marotzke, J., Matei, D., et al. (2013). Characteristics of the ocean simulations in the Max Planck Institute Ocean Model (MPIOM) the ocean component of the MPI-Earth system model. *Journal of Advances in Modeling Earth Systems*, *5*, 422–446. https://doi.org/10.1002/jame.20023

Kargel, J. S., Leonard, G. J., Bishop, M. P., Kääb, A., & Raup, B. H. (2014). *Global land ice measurements from space geophysical sciences*. Berlin Heidelberg: Springer-Verlag.

Kendall, R. A., Mitrovica, J. X., & Milne, G. A. (2005). On post-glacial sea level – II. Numerical formulation and comparative results on spherically symmetric models. *Geophysical Journal International*, *161*(3), 679–706. https://doi.org/10.1111/j.1365-246X.2005.02553.x

Lavallée, D. A., Moore, P., Clarke, P. J., Petrie, E. J., van Dam, T., & King, M. A. (2010). J2: An evaluation of new estimates from GPS, GRACE, and load models compared to SLR. *Geophysical Research Letters*, *37*, L22403. https://doi.org/10.1029/2010GL045229

Martinec, Z., & Hagedoorn, J. (2014). The rotational feedback on linear-momentum balance in glacial isostatic adjustment. *Geophysical Journal International*, *199*(3), 1823–1846. https://doi.org/10.1093/gji/ggu369

Meyrath, T., Rebischung, P., & van Dam, T. (2017). GRACE, era variability in the Earth's oblateness: A comparison of estimates from six different sources. *Geophysical Journal International*, *208*(2), 1126–1138. https://doi.org/10.1093/gji/ggw441

Mitrovica, J. X., & Forte, A. M. (1997). Radial profile of mantle viscosity: Results from the joint inversion of convection and postglacial rebound observables. *Journal of Geophysical Research*, *102*(B2), 2751–2769. https://doi.org/10.1029/96JB03175

Mitrovica, J. X., & Wahr, J. (2011). Ice age Earth rotation. *Annual Review of Earth and Planetary Sciences*, *39*(1), 577–616. https://doi.org/10.1146/annurev-earth-040610-133404

Mohajerani, Y., Velicogna, I., & Rignot, E. (2018). Mass loss of Totten and Moscow University Glaciers, East Antarctica, using regionally optimized GRACE mascons. *Geophysical Research Letters*, *45*, 7010–7018. https://doi.org/10.1029/2018GL078173

Monahan, A. H., Fyfe, J. C., Ambaum, M. H. P., Stephenson, D. B., & North, G. R. (2009). Empirical orthogonal functions: The medium is the message. *Journal of Climate*, *22*(24), 6501–6514. https://doi.org/10.1175/2009JCLI3062.1

Müller Schmied, H., Adam, L., Eisner, S., Fink, G., Flörke, M., Kim, H., et al. (2016). Variations of global and continental water balance components as impacted by climate forcing uncertainty and human water use. *Hydrology and Earth System Sciences*, *20*(7), 2877–2898.

Müller Schmied, H., Eisner, S., Franz, D., Wattenbach, M., Portmann, F. T., Flörke, M., & Döll, P. (2014). Sensitivity of simulated global-scale freshwater fluxes and storages to input data, hydrological model structure, human water use and calibration. *Hydrology and Earth System Sciences*, *18*(9), 3511–3538.

Nerem, R. S., & Wahr, J. (2011). Recent changes in the Earth's oblateness driven by Greenland and Antarctic ice mass loss. *Geophysical Research Letters*, *38*, L13501. https://doi.org/10.1029/2011GL047879

North, G. R. (1984). Empirical orthogonal functions and normal modes. *Journal of the Atmospheric Sciences*, *41*(5), 879–887. https://doi.org/10.1175/1520-0469(1984)041<0879:EOFANM>2.0.CO;2

Peltier, W. R., Argus, D. F., & Drummond, R. (2015). Space geodesy constrains ice age terminal deglaciation: The global ICE-6g_c (VM5a) model. *Journal of Geophysical Research: Solid Earth*, *120*, 450–487. https://doi.org/10.1002/2014JB011176

Rietbroek, R., Brunnabend, S. E., Kusche, J., & Schröter, J. (2012). Resolving sea level contributions by identifying fingerprints in time-variable gravity and altimetry. *Journal of Geodynamics*, *59-60*, 72–81. https://doi.org/10.1016/j.jog.2011.06.007

Rietbroek, R., Brunnabend, S.-E., Kusche, J., Schröter, J., & Dahle, C. (2016). Revisiting the contemporary sea-level budget on global and regional scales. *Proceedings of the National Academy of Sciences*, *113*(6), 1504–1509. https://doi.org/10.1073/pnas.1519132113

Riva, R. E. M., Gunter, B. C., Urban, T. J., Vermeersen, B. L. A., Lindenbergh, R. C., Helsen, M. M., et al. (2009). Glacial isostatic adjustment over Antarctica from combined ICESat and GRACE satellite data. *Earth and Planetary Science Letters*, *288*(3-4), 516–523. https://doi.org/10.1016/j.epsl.2009.10.013

Rodell, M., Houser, P. R., Jambor, U., Gottschalck, J., Mitchell, K., Meng, C.-J., et al. (2004). The global land data assimilation system. *Bulletin of the American Meteorological Society*, *85*(3), 381–394. https://doi.org/10.1175/BAMS-85-3-381

Save, H. (2018). *GRACE RL06 reprocessing and results from CSR*. Austria: EGU General Assembly Vienna.

Scanlon, B. R., Zhang, Z., Save, H., Sun, A. Y., Müller Schmied, H., van Beek, L. P. H., et al. (2018). Global models underestimate large decadal declining and rising water storage trends relative to GRACE satellite data. *Proceedings of the National Academy of Sciences*, *115*, E1080–E1089. https://doi.org/10.1073/pnas.1704665115

Sun, Y., Ditmar, P., & Riva, R. (2016). Observed changes in the Earth's dynamic oblateness from GRACE data and geophysical models. *Journal of Geodesy*, *90*(1), 81–89. https://doi.org/10.1007/s00190-015-0852-y

Sun, Y., Ditmar, P., & Riva, R. (2017). Statistically optimal estimation of degree-1 and C_{20} coefficients based on GRACE data and an ocean bottom pressure model. *Geophysical Journal International*, *210*(3), 1305–1322. https://doi.org/10.1093/gji/ggx241

Sun, Y., Riva, R., & Ditmar, P. (2016). Optimizing estimates of annual variations and trends in geocenter motion and J_2 from a combination of GRACE data and geophysical models. *Journal of Geophysical Research: Solid Earth*, *121*, 8352–8370. https://doi.org/10.1002/2016JB013073

Swenson, S., Chambers, D., & Wahr, J. (2008). Estimating geocenter variations from a combination of GRACE and ocean model output. *Journal of Geophysical Research*, *113*, B08410. https://doi.org/10.1029/2007JB005338

Talpe, M. J., Nerem, R. S., Forootan, E., Schmidt, M., Lemoine, F. G., Enderlin, E. M., & Landerer, F. W. (2017). Ice mass change in Greenland and Antarctica between 1993 and 2013 from satellite gravity measurements. *Journal of Geodesy*, *91*(11), 1283–1298. https://doi.org/10.1007/s00190-017-1025-y

Tamisiea, M. E., Hill, E. M., Ponte, R. M., Davis, J. L., Velicogna, I., & Vinogradova, N. T. (2010). Impact of self-attraction and loading on the annual cycle in sea level. *Journal of Geophysical Research*, *115*, C07004. https://doi.org/10.1029/2009JC005687

Tapley, B. D., Bettadpur, S., Watkins, M., & Reigber, C. (2004). The gravity recovery and climate experiment: Mission overview and early results. *Geophysical Research Letters*, *31*, L09607. https://doi.org/10.1029/2004GL019920

Thomas, M. (2002). Ocean induced variations of Earth's rotation results from a simultaneous model of global circulation and tides (PhD thesis), University of Hamburg, Germany.

Wahr, J., Nerem, R. S., & Bettadpur, S. V. (2015). The pole tide and its effect on GRACE time-variable gravity measurements: Implications for estimates of surface mass variations. *Journal of Geophysical Research: Solid Earth*, *120*, 4597–4615. https://doi.org/10.1002/2015JB011986

Yoder, C. F., Williams, J. G., Dickey, J. O., Schutz, B. E., Eanes, R. J., & Tapley, B. D. (1983). Secular variation of Earth's gravitational harmonic J_2 coefficient from Lageos and nontidal acceleration of Earth rotation. *Nature*, *303*(5920), 757–762. https://doi.org/10.1038/303757a0

Zhang, H., & Sun, Y. (2018). Climate-driven seasonal geocenter motion during the GRACE period. *Acta Geophysica*, *66*(2), 223–232. https://doi.org/10.1007/s11600-018-0130-5

Zwally, H. J., Giovinetto, M. B., Beckley, M. A., & Saba, J. L. (2012). Antarctic and Greenland drainage systems. GSFC Cryospheric Sciences Laboratory.